



RESEARCH ARTICLE

10.1029/2023JD038509

Key Points:

- Because sufficiently large haze particles can be misinterpreted as droplets, mixing can appear more homogeneous
- Solute and curvature effects initiate microphysical changes (Ostwald ripening) that can be confounded with inhomogeneous mixing
- Haze particles are shown to buffer the negative impacts of inhomogeneous mixing on the cloud albedo

Correspondence to:

F. Hoffmann,
fa.hoffmann@lmu.de

Citation:

Kainz, J., & Hoffmann, F. (2023). The effects of aerosol on small-scale cloud-environment mixing: Implications for simulating and observing inhomogeneous mixing. *Journal of Geophysical Research: Atmospheres*, 128, e2023JD038509. <https://doi.org/10.1029/2023JD038509>

Received 9 JAN 2023
Accepted 30 OCT 2023
Corrected 20 DEC 2023

This article was corrected on 20 DEC 2023. See the end of the full text for details.



Author Contributions:

Conceptualization: Johannes Kainz, Fabian Hoffmann
Data curation: Johannes Kainz
Formal analysis: Johannes Kainz
Funding acquisition: Fabian Hoffmann
Investigation: Johannes Kainz, Fabian Hoffmann
Methodology: Johannes Kainz, Fabian Hoffmann
Project Administration: Fabian Hoffmann
Resources: Johannes Kainz
Software: Johannes Kainz, Fabian Hoffmann
Supervision: Fabian Hoffmann

© 2023. The Authors.

This is an open access article under the terms of the [Creative Commons Attribution License](https://creativecommons.org/licenses/by/4.0/), which permits use, distribution and reproduction in any medium, provided the original work is properly cited.

The Effects of Aerosol on Small-Scale Cloud-Environment Mixing: Implications for Simulating and Observing Inhomogeneous Mixing

Johannes Kainz¹  and Fabian Hoffmann¹ 

¹Meteorological Institute, Ludwig-Maximilians-Universität München, München, Germany

Abstract Entrainment-mixing modulates the number and size of cloud droplets, and thus affects the optical properties of clouds and their role in the climate system. Using a statistical turbulence model coupled with Lagrangian cloud microphysics, we analyze the role of aerosol in the entrainment-mixing process, which, for instance, prevent the full evaporation of cloud droplets, leaving behind haze particles. To test a commonly applied indicator for inhomogeneous mixing, a set of different mixing scenarios is simulated. We conclude that if a hard separation radius between cloud droplets and haze particles is chosen, the typical classification into homogeneous and inhomogeneous mixing can be wrong because larger haze particles might be misidentified as cloud droplets, making the mixing appear more homogeneous. Furthermore, we show that the growth of cloud droplets on the expense of other hydrometeors due to differences in aerosol loading and particle curvature (Ostwald ripening) can produce cloud microphysical signatures indistinguishable from inhomogeneous mixing. Finally, we investigate how the consideration of haze particles can mitigate the previously reported negative impacts of inhomogeneous mixing on the cloud albedo. These findings should be considered when interpreting observations and simulations of small-scale entrainment-mixing.

Plain Language Summary The mixing of clouds with their environment can change the size and number of cloud droplets, two important parameters to understand the role of clouds in the climate system. Because these changes are determined by the specific way a cloud mixes with its environment, they have traditionally been used to characterize the mixing process. Using a highly detailed numerical cloud modeling framework, we show that the adequate consideration of aerosol particles from which cloud droplets grow can alter the actual and apparent changes of cloud droplets during mixing. We identify biases that need to be considered when mixing is analyzed in observations and simulations.

1. Introduction

Although ongoing progress has been made to understand the Earth's climate system, the role of clouds is still shrouded. The role of clouds cannot be simplified to one single effect but is determined by the continuous interplay of various mechanisms ranging from the interaction of individual cloud droplets and aerosol particles up to the global circulation, influencing the hydrological cycle and the global radiation budget. Here, stratocumulus clouds are of great importance since they exert a strong negative, that is, cooling, forcing on the climate system (Masson-Delmotte et al., 2021).

Stratocumulus are typically found at the top of a cold and moist marine boundary layers, into which warm and dry air from the free troposphere above is entrained and eventually mixed. This mixing process occurs in a turbulent manner, where the exchange between the cloud-free troposphere and the stratocumulus-topped boundary layer happens by thermally driven motions that engulf filaments of the dry air that are dragged, deformed, and diluted. Therefore, the exposure of cloud droplets to the entrained air varies both temporally and spatially, and each particle has its individual growth or evaporation history (e.g., Krueger & Tölle, 2014; Lasher-Trapp et al., 2005).

The evaporation of cloud droplets exposed to the free-tropospheric air is imagined to take one of two limiting pathways (e.g., Baker & Latham, 1979). The first is called homogeneous mixing, which reduces the liquid water content (LWC) by evaporating all cloud droplets partially, that is, reducing their size but not their number concentration (N_c). In the second limit of extreme inhomogeneous mixing, the opposite happens. The LWC is reduced by evaporating individual droplets completely, while leaving other droplets unblemished. Thus, N_c decreases, but

Validation: Fabian Hoffmann
Visualization: Johannes Kainz
Writing – original draft: Johannes Kainz
Writing – review & editing: Fabian Hoffmann

not the mean cloud droplet size. It is important to note that in both cases N_c will decrease by the dilution caused by the mixing with entrained air.

The concept of inhomogeneous mixing dates back 40 years, when it was realized that mixing is not happening instantaneously and hence homogeneously (Baker & Latham, 1979; Baker et al., 1980; Latham & Reed, 1977). But the confusion about the character of the entrainment-mixing process is almost as old as well. Not only exist opinions that support both ideas, that is, the entrainment-mixing process is either predominately homogeneous or inhomogeneous, but also estimates on their effects vary substantially. For instance, if small-scale mixing was inhomogeneous, interactions of the cloud and its environment must be resolved on scales as small as a few decimeters for an adequate representation in numerical models (e.g., Lehmann et al., 2009), causing a substantial computational burden. Furthermore, a study by Chosson et al. (2007) found that in fragmented, thin stratocumulus clouds the assumption of extreme inhomogeneous over homogeneous mixing can cause an albedo bias of up to -31% .

Such uncertainties urge the need for a robust classification tool for small-scale mixing processes. One commonly used approach is the cloud microphysical mixing diagram that juxtaposes the changes in N_c and droplet size to determine the mixing character (Burnet & Brenguier, 2007). However, this approach might be limited by its idealized representation of cloud microphysics, as we will detail in this study. For example, the mixing diagram does not consider that cloud droplets never fully evaporate, but leave behind an aqueous aerosol particle, often referred to as haze.

Distinguishing between cloud droplets and haze is not always possible. While Köhler theory provides a theoretical framework for this (Köhler, 1936), the necessary simultaneous measurement of the aerosol and liquid water masses in a single aqueous particle is practically impossible in real clouds. Furthermore, haze particles also contribute non-negligibly to the cloud radiative forcing (Hoffmann et al., 2022), potentially buffering the aforementioned negative impacts of inhomogeneous mixing. The solute aerosol contained in every cloud droplet can also impact the development of the entire droplet size distribution in ways that might interfere with the effects of mixing by also evaporating parts of the droplet ensemble (Korolev, 1995).

Inspired by these additional constraints, we want to address how aerosol changes our understanding of the mixing process, its detectability, and effects. Particularly, we want to answer the following questions:

- What is the role of aerosol in the small-scale mixing processes?
- Is the mixing character affected by the definition of cloud and haze particles?
- When do optical effects caused by the haze particles become relevant?

The paper is organized as follows. First, we summarize the relevant theoretical concepts, as well as the computational model and its setup used in this study (Sections 2–4). Then, the results are presented, focusing on the three aforementioned leading questions (Section 5). Finally, the paper is concluded (Section 6).

2. Theoretical Preliminaries

2.1. Köhler Theory

Since all the considerations made in this study are based on a clear notion to distinguish haze from cloud particles, it is necessary to discuss the underlying theoretical framework used to make this separation.

A cloud droplet is formed when sufficient water vapor condenses on an aerosol particle that acts as a so-called cloud condensation nucleus. This process is governed by Köhler theory, which predicts the saturation necessary for a solution droplet to be in equilibrium with its environment, such that the particle neither evaporates nor grows by condensation (Köhler, 1936). The corresponding saturation ratio is

$$S_k = \frac{A}{r_d} - \frac{B}{r_d^3}, \quad (1)$$

where r_d is the liquid radius of the solution droplet, A accounts for the curvature of the particle, B describes the solute effect that is dictated by the soluble substances that form the aerosol particle. Note that B is proportional to the mass of solute aerosol. The definitions of A and B follow Rogers and Yau (1989). The maximum of S_k , the critical supersaturation $S_{crit} = \sqrt{4A^3/(27B)}$, is reached for $r_d = \sqrt{3B/A} \equiv r_{crit}$, the critical radius. Only if the

ambient supersaturation S exceeds S_{crit} , a cloud droplet can develop. Thus, if $r_d > r_{\text{crit}}$, a particle is considered activated and is commonly called a cloud droplet. If $r_d < r_{\text{crit}}$, the particle is not activated and considered haze.

2.2. The Damköhler Number

A common approach to diagnose the mixing character of an entrainment event is the Damköhler number

$$\text{Da} = \frac{\tau_{\text{mixing}}}{\tau_{\text{evap}}}. \quad (2)$$

Da considers the turbulent mixing timescale

$$\tau_{\text{mixing}} = \left(\frac{l^2}{\epsilon} \right)^{\frac{1}{3}}, \quad (3)$$

which is a measure of the time to homogenize a filament of entrained air of the characteristic size l with the cloud at a kinetic energy dissipation rate ϵ . Furthermore, Da depends on the time to fully evaporate a droplet of size r_d , given by

$$\tau_{\text{evap}} = r_d^2 \frac{F_k + F_D}{2|S|}, \quad (4)$$

with F_k and F_D being parameters depending on heat conduction and molecular diffusion of water vapor, which stem from the diffusional growth Equation 8 further detailed in Section 3 below. Here, $S < 0$ is the (negative) ambient supersaturation experienced by the droplet. Based on this definition, $\text{Da} \ll 1$ predicts homogeneous mixing because the mixing tends to be finished before evaporation, and thus all droplets experience a similar subsaturation, and $\text{Da} \gg 1$ predicts inhomogeneous mixing where the mixing is so slow that only those droplets that move into the subsaturated air of the entrained filament evaporate (e.g., Lehmann et al., 2009).

While this method is theoretically sound, it cannot be applied directly to measurements or large-eddy simulation data since it is nearly impossible to determine l . In the setup presented in this paper, l is known as an initialization parameter, and Da can be determined easily.

2.3. The Degree of Inhomogeneity in Small-Scale Mixing

Small-scale mixing in warm clouds can occur in different qualitative manifestations, depending on, inter alia, cloud microphysical composition, strength of turbulence, and the thermodynamic properties of the cloudy and entrained air. One measure to quantify small-scale mixing is the inhomogeneous mixing degree (IHMD) (Andrejczuk et al., 2009; Lu, Liu, et al., 2013; Lu, Niu, et al., 2013), which evolved from the microphysical mixing diagram (Burnet & Brenguier, 2007).

The IHMD is used to characterize the mixing behavior on a spectrum between the boundaries of homogeneous and extreme inhomogeneous mixing. Because the mixing type does not affect the LWC after mixing, all possible combinations of N_c and the volume mean radius $r_v = [3\text{LWC}/(4\pi\rho_l N_c)]^{\frac{1}{3}}$, with ρ_l the mass density of liquid water, can be expressed as

$$\text{LWC} \propto r_v^3 N_c = r_{v,h}^3 N_{c,h} = r_{v,i}^3 N_{c,i} = \text{const.}, \quad (5)$$

where the subscripts h and i indicate the corresponding values for homogeneous or extreme inhomogeneous mixing, respectively. Note that observations often use adiabatic values to deduce $r_{v,h}$, $r_{v,i}$ and $N_{c,h}$ (e.g., Korolev et al., 2016). By generalizing expression (5) as

$$\frac{N_c}{N_{c,h}} = \left(\frac{r_{v,h}^3}{r_{v,i}^3} \right)^{\text{IHMD}}, \quad (6)$$

we get

$$\text{IHMD} = \frac{\ln(N_c/N_{c,h})}{\ln(r_{v,h}^3/r_{v,i}^3)} = \frac{\ln\{N_c/[(1-f_\epsilon)N_{c,0}]\}}{\ln\{(r_v^3 N_c)/[(1-f_\epsilon)r_{v,0}^3 N_{c,0}]\}}, \quad (7)$$

which describes the full range of mixing scenarios from homogeneous mixing (IHMD = 0) to extreme inhomogeneous mixing (IHMD = 1) (Andrejczuk et al. (2009), Lu, Liu, et al. (2013)). As N_c is the only free parameter in the IHMD, we see already that any changes in N_c will have an impact on the diagnosed IHMD. In Equation 7, the IHMD is determined from the initial droplet size distribution, indicated by the subscript 0, and the current values. The factor $1 - f_c$ is necessary to account for the dilution of the cloud by entrained air, occupying the fraction f_c of the cloud.

3. Modeling Approach

We apply a detailed Lagrangian cloud microphysics model (LCM) fully coupled to a one-dimensional stochastic turbulence model, the Linear Eddy Model (LEM). The interested reader is referred to Hoffmann et al. (2015) for details on the LCM, Kerstein (1988) on the LEM, and Hoffmann (2020) on the coupling of the two models. Here, we summarize the basic features of the applied modeling framework.

In the LEM, turbulent convection is represented by individual eddies that are stochastically sampled over the whole domain, using inertial range scaling. The individual eddies are implemented by an approach first described by Kerstein (1988), based on the rearrangement of all predicted scalar quantities (water vapor mixing ratio and absolute temperature) by performing a slicing, compression, and folding action that mimics turbulence, followed by molecular diffusion. In the LEM domain this is done by stochastically reshuffling grid boxes along the one dimension of the LEM during each timestep, as can be seen in Figure 1. It is important to note that by using the LEM, the exchange of water vapor, temperature, and their interaction with individual hydrometeors is determined by the turbulent character of the mixing process, which is primarily prescribed by ϵ and an outer scale of turbulence, which is identical to the LEM domain size in this study. Entrainment in the LEM is considered by replacing a fraction of the domain by air with different thermodynamical properties. For this study, we assume that the LEM is oriented vertically, and the domain is assumed to exhibit cyclic boundaries. Note that vertical motions in the LEM cause fluctuations in temperature and hence in S (Hoffmann, 2020).

The defining feature of the LCM is that cloud microphysics are represented by individually simulated cloud droplets or haze particles, predicting, for example, their position in the LEM and changes in water mass. For this, the diffusional growth equation,

$$r_d \frac{dr_d}{dt} = \frac{1}{F_K + F_D} (S - S_k), \quad (8)$$

is solved for every particle, predicting changes in r_d by considering Köhler theory via S_k explicitly. Here, S is determined in the LEM. Condensation and evaporation predicted from Equation 8 feed back to the temperature and water vapor in the LEM. Note that the LCM does not artificially discriminate between cloud droplets and haze particles. Their different behavior is naturally considered via S_k in Equation 8. The location of each LCM particle in the LEM is determined by integrating its vertical velocity

$$w = w_{\text{LEM}} + w_{\text{sedi}}(r_d), \quad (9)$$

where w_{LEM} is the particle's relocation due to the LEM and w_{sedi} the sedimentation velocity of the particle, primarily determined by its size (Beard, 1976).

4. Physical Setup

As stratocumulus exhibit comparably low turbulence, making inhomogeneous mixing more likely, we chose this cloud type to set up our simulations. Those clouds cover mixing processes on multiple spatial scales, covering the small-scale interactions of cloud microphysics and turbulence to the large scales driving the dynamics of the boundary layer (Lilly, 1968; Mellado, 2017). Small-scale mixing events are mainly driven by turbulence and dominate the stratocumulus top, where dry free-tropospheric air is mixed with the humid cloudy air, which is transported deeper into the cloud by the large-eddy circulation processes (Yamaguchi & Randall, 2012). A characteristic feature of the inversion at the top of the cloud layer is the strong increase in temperature and decrease in humidity toward the free troposphere (Wood, 2012). In this stably stratified environment, small-scale mixing plays a crucial role to decrease the positive buoyancy of the free-tropospheric air that will be entrained eventually.

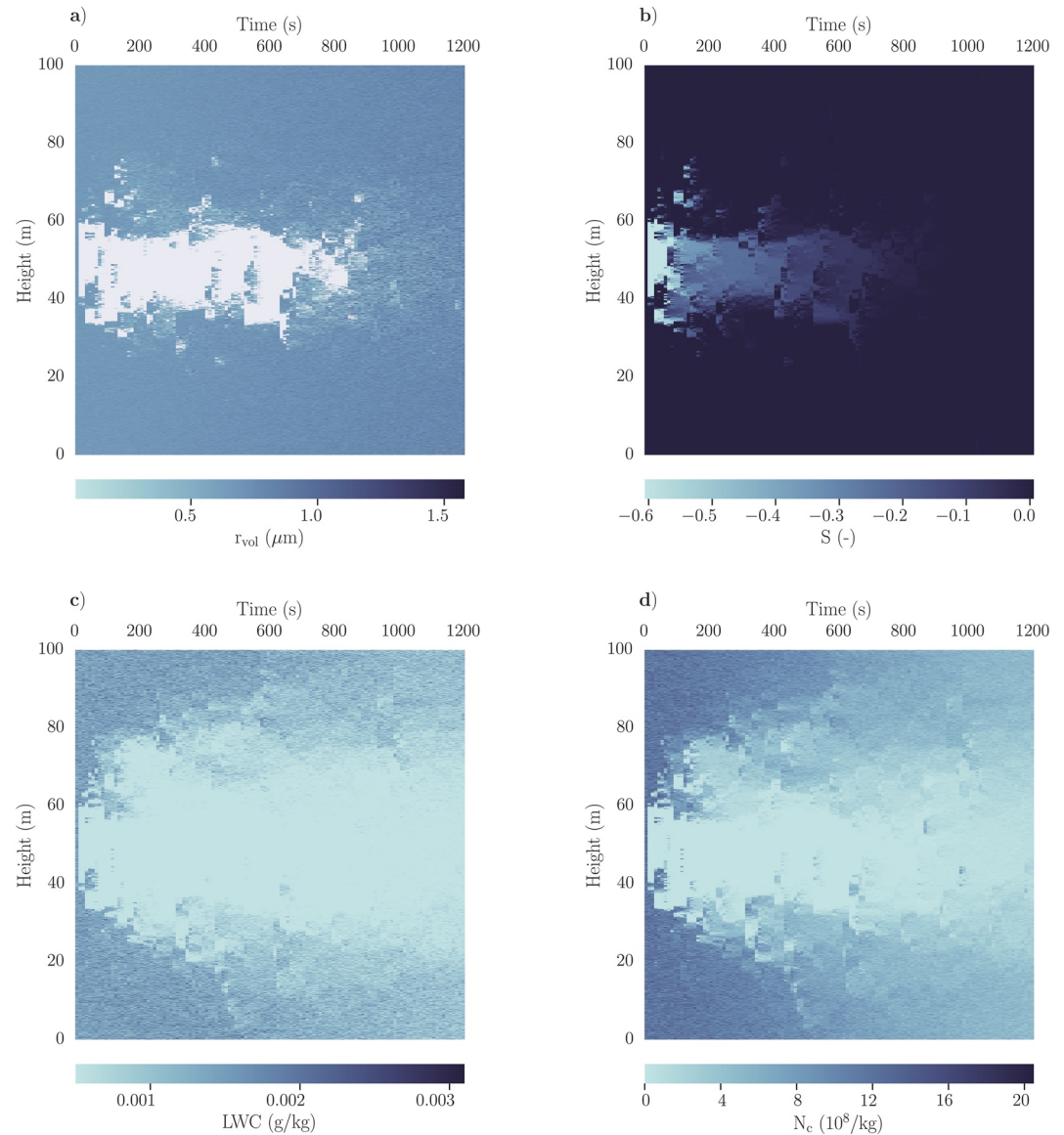


Figure 1. Time evolution of (a) r_{vol} , (b) S , (c) liquid water content, and (d) N_c in the model domain. A single run with $e = 10 \text{ cm}^2 \text{ s}^{-3}$, $N_c = 1158 \text{ cm}^{-3}$, and $r_{mean,a} = 25 \text{ nm}$ is shown.

This interplay of small- and large-scale mixing processes interacting with cloud microphysics at the top of stratocumulus clouds sets the stage how we initialize the LEM-LCM modeling framework. The LEM domain is 100 m with a total of 10,000 grid boxes, resulting in a vertical resolution of 1 cm. The vertical orientation of the model is necessary for enabling fluctuations in S due to turbulent vertical motions. To understand the influence of sedimentation, additional runs excluding particle sedimentation have been performed. The result show no substantial differences. Because the Kolmogorov lengthscale is not resolved, molecular diffusion is scaled to account for the unresolved turbulent mixing on the scales below 1 cm. In the context of small-scale cloud-environment mixing, an idealization of those scales is sufficient, since small-scale cloud-environment mixing tends to homogenize on scales of around 10 cm (e.g., Lehmann et al., 2007). The timestep of LEM and LCM is 0.1 s and subcycled when necessary. The total runtime of all simulations is set to 1,200 s ensuring that in all simulations mixing is completed before the simulation ends.

Note that in the LCM applied here, each computational particle represents one hydrometeor, that is, one cloud droplet or haze particle. The LCM particles are randomly placed in the LEM domain. The initial droplet size distribution is produced by randomly assigning each LCM particle a liquid radius from a lognormal distribution

Table 1
Physical Input Parameters of the 36 Configurations Used in This Study

N_c (cm ⁻³)	$r_{\text{mean,a}}$ (nm)	ϵ (cm ² s ⁻³)	$r_{\text{mean,d}}$ (μm)
57	25.0	1.0	15.7
193	50.0	10.0	10.5
386	100.0	100.0	8.4
1,158			5.9

function, with a geometric standard deviation of 1.36 typical for cloud droplet spectra (e.g., Geoffroy et al., 2010), and a geometric mean radius, which is adapted to keep the LWC constant for all the different N_c considered in this study. The LWC is initialized such that it reaches 0.6 g kg⁻¹ after mixing is finished, a value which corresponds to an adiabatic cloud depth of 300 m, which is common for subtropical stratocumulus (Wood, 2012). The initial droplet concentration N_c is varied between 57, 193, 386, and 1,158 cm⁻³, covering a spectrum from moderately clean to highly polluted clouds (Wood, 2012). The resultant initial geometric mean droplet radii $r_{\text{mean,d}}$ vary between 15.7, 10.5, 8.4, and 5.9 μm, respectively.

The underlying dry aerosol is also log-normally distributed with mean geometric radii $r_{\text{mean,a}}$ varied between 25, 50, and 100 nm, has a constant geometric standard deviation of 1.36, and is assumed to consist of sodium chloride (NaCl). The dry aerosol radii are randomly assigned to each droplet such that there is no correlation between dry aerosol and liquid radius initially. Note that the underlying dry aerosol sizes cover a realistic range found in maritime and continental environments (Jaenicke, 1993).

The LEM is initially saturated (relative humidity of 100%) at a temperature of 15°C and a hydrostatic pressure of 950.5 hPa, typical for a subtropical stratocumulus. The fraction of replaced air by the initial entrainment event is $f_e = 0.2$, but increased later to 0.3 for the optical properties study. The relative humidity of the entrained air is 40%, reflecting the thermodynamic conditions in the free troposphere above the cloud layer. The temperature of the entrained air is only 2 K warmer than the cloud, which is slightly less than the typical difference between the temperature at the top of stratocumulus and the free troposphere. All aerosol particles are assumed to be haze particles initially, as deliquescence and efflorescence is not considered in our model. The liquid radius of the LCM particles in the entrained air is adjusted to be in equilibrium with their initial environment. The entrained dry aerosol distribution is identical to the distribution inside the cloud. To represent various turbulent conditions, ϵ is varied between 1, 10, and 100 cm²s⁻³, where 10 cm²s⁻³ is typical for stratocumulus clouds (Xue et al., 2008). Note that the degree of turbulence is prescribed in the LEM, and does not change in the course of the simulation. Typically, one would expect a slight increase in turbulence during mixing, driven by evaporative cooling, and a decrease afterward (e.g., Kumar et al., 2014). Large-scale vertical motions of the entire LEM are neglected. For each of the 36 configurations in Table 1, we simulated an ensemble of 100 individual runs, each one with a randomly generated initial microphysical state in the LCM, and a different realization of turbulence in the LEM.

5. Results

Figure 2 shows the temporal development of the simulated entrainment event. The entrainment creates an initially subsaturated zone in the otherwise saturated cloud, causing the domain mean to be subsaturated (Figure 2a). Due to the turbulent mixing, cloud droplets get moved into subsaturated regions, where they evaporate and deactivate, causing the LWC and N_c to decrease (Figures 2b and 2c), while the saturation ratio increases due to the release of water vapor (Figure 2a). Note that the number concentration of haze particles N_a increases (Figure 2d), balancing the losses in N_c . We see that the velocity with which the domain saturates is proportional to ϵ (line thickness), which enables a faster mixing of the cloud with the entrained air. Furthermore, the saturation process is accelerated for larger N_c (warmer line colors) because the larger integral droplet surface area enables a faster release of water vapor through evaporation, which is most visible for large ϵ (thick lines). For small ϵ (narrow lines), however, small N_c runs saturate earlier (colder line colors). This is because of the larger droplets that sediment into the subsaturated air where they evaporate. Together, the dependency on ϵ and N_c indicates that the mixing process is not only determined by turbulence but also the microphysical composition of the cloud. For the following analysis, we will define the end of the mixing process as the moment in which saturation is reached and the LWC starts to remain constant. The end of the mixing process is also reflected in Figure 2e, showing the relative dispersion of water vapor σ_q/\bar{q} in the LEM domain, which reaches a steady state at a similar time as S and LWC. Generally, the mixing tends to be finished after 200 s in the high ϵ runs and after 1,000 s for low ϵ . Note that even when the mixing is finished, there is still an increase in N_a and a decrease in N_c , a process that will be analyzed in more detail below.

Figures 2f and 2g show the effective radii for the haze particles, $r_{\text{eff,a}}$, and the cloud droplets, $r_{\text{eff,d}}$, which are defined as the ratio of the third to the second moment of the respective particle size distribution. While $r_{\text{eff,d}}$ is mainly controlled by N_c (line color), determining how much water is assigned to each droplet, $r_{\text{eff,a}}$ is primarily controlled by the mean aerosol radius (line pattern), reflecting how haze particles assume their equilibrium radius

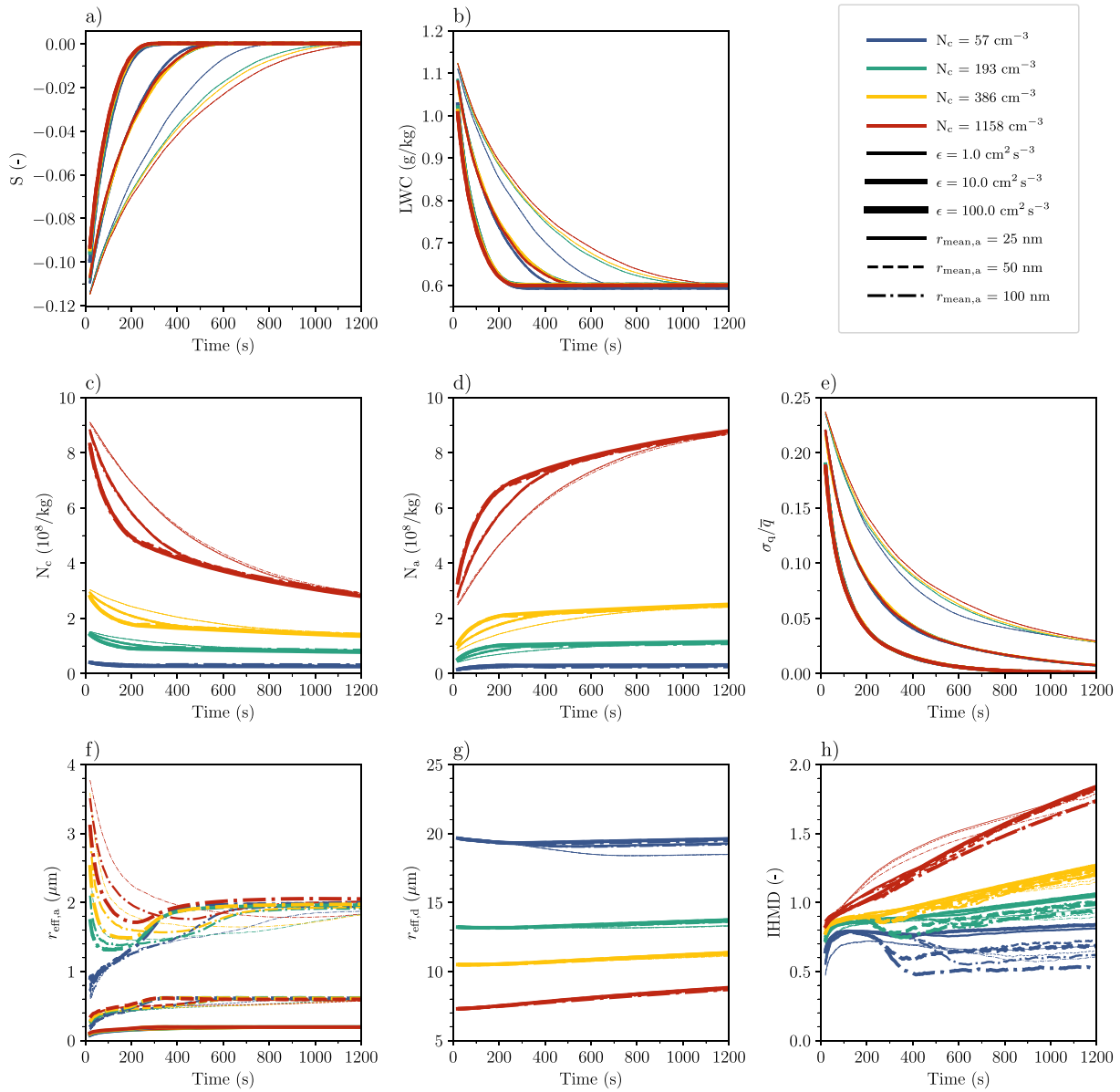


Figure 2. Time evolution of the domain-averaged, that is, arithmetic mean of all grid boxes, (a) S , (b) liquid water content, (c) N_a , (d) N_c , (e) water vapor relative dispersion σ_q/q , (f) $r_{\text{eff},a}$, (g) $r_{\text{eff},d}$, and (h) inhomogeneous mixing degree for various initial and boundary conditions (line color, pattern, and thickness).

which is mainly determined by the amount of solute aerosol in saturated conditions (e.g., Sedunov et al., 1974). During the mixing ($t < 200$ s), $r_{\text{eff},d}$ slightly decreases for low N_c (blue lines), which is indicative of more homogeneous mixing. For higher N_c , $r_{\text{eff},d}$ is constant (green and yellow lines) or even slightly increases (red lines), which is indicative of an inhomogeneous mixing process. To understand this unexpected behavior, note that $r_{\text{eff},d}$ is determined from the third and second moment of the droplet size distribution, compared to, for example, the arithmetic mean radius (first moment of the droplet size distribution), which explains why despite notable changes in N_c (Figure 2c) there are only small variations in $r_{\text{eff},d}$ (Figure 2g).

5.1. How the Inhomogeneous Mixing Degree Depends on the Separation Between Cloud Droplets and Haze Particles

For the above-discussed cases, the character of the mixing process is determined using the IHMD (Figure 2h). The IHMD is determined using Köhler theory to distinguish between haze particles and cloud droplets.

First, we see a distinct increase in the IHMD from more homogeneous to more inhomogeneous mixing during the initial phase of the mixing process ($t < 100$ s). This increase is especially strong for low N_c and hence large droplets (blue lines), which require some time for evaporation and thus favor homogeneous mixing. After inhomogeneous mixing has been fully developed ($t > 200$ s), the mixing becomes more homogeneous again, which is expected due to the almost saturated environment (Figure 2a), which slows down microphysical reactions. Note, however, that although there is no mixing of cloud and cloud-free air for $t \gg 200$ s, the IHMD interprets the continuing cloud microphysical changes as inhomogeneous mixing. In fact, the IHMD exceeds 1, that is, becomes larger than the limit for extreme inhomogeneous mixing for the high N_c cases (red lines). This will be dealt with in Subsection 5.2.

Overall, the impact of ϵ on the IHMD is not as severe as expected (line thickness). On the other hand, the initial N_c (line color) has a big impact on the degree of inhomogeneity because smaller droplets tend to evaporate faster, which favors more inhomogeneous mixing scenarios (Baker & Latham, 1979). To verify the inhomogeneous mixing characteristics described by the IHMD, Da has been calculated for all configurations (τ_{mixing} ranging from 7.4 to 5,130.0 s and τ_{evap} from 0.5 to 3.6 s), resulting in Da between 2 and 10,260, that is, inhomogeneous to extreme inhomogeneous mixing. Therefore, we see a general agreement of IHMD and Da for the mixing until $t < 200$ s.

In our simulations, we are able to determine if a particles is a cloud droplet or a haze particle by considering its dry aerosol mass and Köhler theory. This is usually not possible in measurements, where the dry aerosol radius is unknown. Thus, a fixed separation radius is often applied to constrain the spectrum of cloud droplets and hence N_c . To investigate the impact of this approach, we also used a radius of 1 μm to separate between cloud droplets and haze particles in the previously presented simulations. The effect on the IHMD and N_c is shown in Figures 3a and 3b. The IHMD still exceeds the limit for extreme inhomogeneous mixing (IHMD = 1) for several configurations. However, we see a much higher sensitivity to ϵ . Overall, however, the cases are more homogeneous, which is an effect caused by overestimating N_c . Especially the larger aerosol particles (dash-dotted lines) have an $r_{\text{crit}} > 1$ μm , that is, droplets deactivate at larger radii than the artificial separation radius applied here. Thus, homogeneous mixing is predicted, because those particles are erroneously counted as cloud droplets.

To determine the severity of this effect for a wider range of separation radii, Figure 3c shows the IHMD for separation radii between 0.25 and 2 μm , as well as the IHMD determined from Köhler theory for different dry aerosol mean radii (dot and line colors, respectively). For this plot, only a subset of the produced data is shown for clarity. Ensembles with $\epsilon = 10 \text{ cm}^2 \text{ s}^{-3}$ and $N_c = 193 \text{ cm}^{-3}$ have been chosen, representing a typical stratocumulus environment and exhibiting almost similar mixing behaviors for all investigated aerosol radii (cf. Figure 2). Nonetheless, to make the different simulations more comparable with regard to their mixing, the presented IHMDs are obtained at $S = -0.05$, rather than a specific time. By comparing the IHMD for a given separation radius to the IHMD from Köhler theory, we find deviations of up to 85% for the smallest separation radii. The deviations tend to decrease for larger separation radii. Fixed separation radii underestimate the IHMD strongest when the aerosol mean radius is large (blue dots) because too many haze particles are misinterpreted as cloud droplets. By increasing the separation radius to 2 μm , the bias in estimating the IHMD can be eliminated. However, many instruments used to measure cloud droplet spectra use minimum radii of, for example, 0.2 μm for the cloud-aerosol spectrometer (CAS) (e.g., Baumgardner et al., 2001), 0.7 μm for the forward scattering spectrometer probe (FSSP) (Brenner et al., 1993), or 1.5 μm for the particulate volume monitor (PVM) (Gerber et al., 1994), making them susceptible to this bias.

Figure 3d shows the particle size distributions corresponding to Figure 3c. We clearly see that the haze and cloud droplet modes are separated by a minimum around 1 μm . However, if larger aerosol sizes are prescribed (blue line), the minimum is not as distinct as for small aerosol sizes (red line). The reason for these changes are the larger equilibrium radii of the haze particles grown from larger aerosol particles. This clearly indicates that an IHMD determined by a separation radius has the tendency to overestimate homogeneous mixing if the background aerosol contains larger particles, as is most likely the case for maritime environments where sea spray tends to add larger salt aerosol particles to the atmosphere (Jaenicke, 1993).

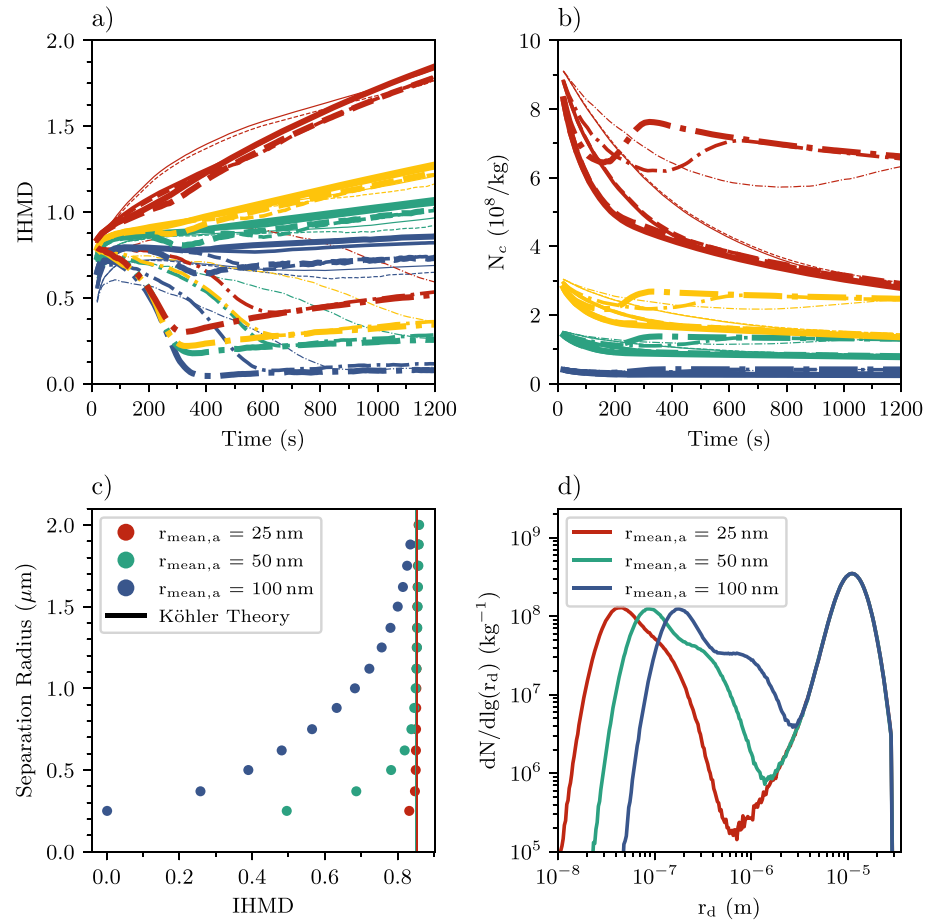


Figure 3. The inhomogeneous mixing degree (IHMD) (a) and N_c (b) from the simulations presented in Figure 2, using a separation radius of 1 μm to discriminate between cloud droplets and haze particles. See Figure 2 for line labels. (c) Comparison of the IHMD determined using various separation radii (dots) or Köhler theory (lines). Here, only results for $\epsilon = 10 \text{ cm}^2 \text{ s}^{-3}$ and $N_c = 193 \text{ cm}^{-3}$ are shown. The IHMD is determined at $S = -0.05$. Note that the three different lines for Köhler theory overlap. (d) Particle size distributions at $S = -0.05$ for different mean aerosol sizes, but the same $\epsilon = 10 \text{ cm}^2 \text{ s}^{-3}$ and $N_c = 193 \text{ cm}^{-3}$.

5.2. Ostwald Ripening

In the section above, we have seen a substantial increase in the IHMD over time, even in the absence of mixing, that is, after a saturated environment is reached ($>200 \text{ s}$ depending on ϵ , Figures 2h and 3a). As we will show here, this is due to the solute and curvature terms, that is, Köhler theory, considered in the diffusional growth Equation 8. Thus, we compiled a set of simulations without taking into account the Köhler terms ($S_k = 0$). Consequently, cloud droplets and haze particles had to be separated by a separation radius. Here, we chose 1 μm .

Figure 4a shows that the increasing trend in IHMD disappears after mixing ($t > 200 \text{ s}$), while the qualitative behavior during the mixing ($t < 200 \text{ s}$) is similar. This is a hint that turbulent mixing is a more dominant process than the solute and curvature effects during the actual mixing event. But when the mixing fades out, the solute and curvature effects are dominating and cause changes in the droplet size distribution when Köhler theory is considered (Figure 2). The positive slope of the IHMD in Figure 2h can therefore be explained by a decrease in N_c while r_v^3 increases. Large particles continue to grow on expense of smaller ones. This causes the deactivation of small particles as they shrink below their critical radius (Figures 2c and 2d). In fact, without Köhler theory, N_c remains almost constant after mixing (Figure 4b).

The behavior contrasted in Figures 2 and 4, frequently called Ostwald ripening, is one of the consequences of Köhler theory: Consider two droplets of identical size but different aerosol loading experiencing the same saturation. The droplet grown on the smaller aerosol particle will evaporate due to a smaller solute effect, while

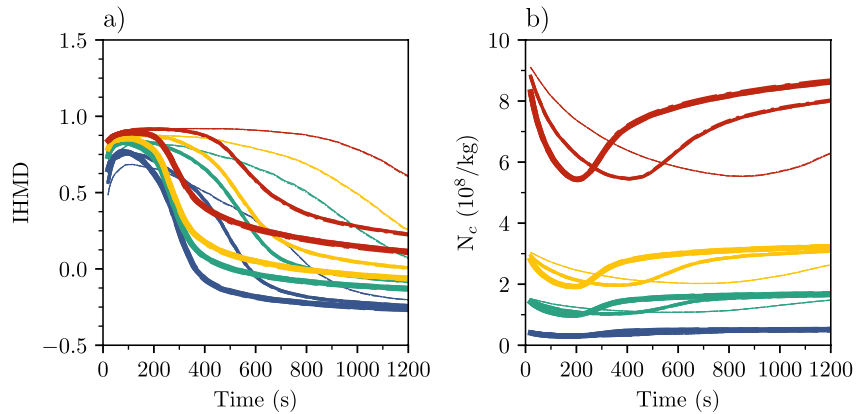


Figure 4. The inhomogeneous mixing degree (a) and N_c (b) without Köhler theory [$S_k = 0$ in Equation 8], and a fixed separation radius of $1 \mu\text{m}$ to discriminate between cloud droplets and haze particles.

the droplet grown on the larger aerosol will grow from the water vapor released by the first droplet (Çelik & Marwitz, 1999; Hagen, 1979; Korolev, 1995; Wood et al., 2002). This effect becomes more severe for higher particle concentrations, where the mean S tends to be lower and droplets are smaller, causing a larger number of particles to be affected by the solution and curvature effects of Köhler theory. This analysis shows that Ostwald ripening causes cloud microphysical reactions that could be mistaken for inhomogeneous mixing. Moreover, the effect is especially strong for droplet-laden environments where we expect more inhomogeneous mixing. Thus, conclusions on the mixing character have to consider the possibility of Ostwald ripening producing a similar effect. Moreover, this effect is most likely to occur at the top of stratocumulus where entrainment and mixing take place, and S is small because of the absence of substantial vertical motions, which increases the relative importance of the Köhler terms on diffusional growth. At lower levels of the cloud, stronger vertical motions cause higher S , which might allow all droplets to grow, limiting the effects of Ostwald ripening.

5.3. Optical Properties

The previous subsections have shown that the consideration of aerosol can have substantial implications for the observed mixing character. But do these particles also affect the optical properties of a cloud? Chosson et al. (2007) showed that extreme inhomogeneous mixing can cause an albedo bias of up to -31% . They, however, neglected the presence of haze particles.

Because determining the cloud albedo for the applied modeling framework requires rather arbitrary choices, we will determine the effective extinction instead, which can be expressed as

$$\beta_{\text{ext}} = \int [1 - g(r_d, \lambda)] Q_{\text{ext}}(r_d, \lambda) \pi r_d^2 n(r_d) dr_d, \quad (10)$$

where g is the asymmetry parameter, Q_{ext} the extinction coefficient, and n the particle size distribution. Here, a wavelength of $\lambda = 500 \text{ nm}$, representative of the bulk of solar shortwave radiation, is used. g and Q_{ext} are determined from parameterizations by Mitchell (2000) and Kokhanovsky (2004), respectively, which consider Mie effects, necessary for small particles with $r_d \leq \lambda/(2\pi)$. Note that β_{ext} relates to the cloud optical thickness via its vertical integral, $\tau_c = \int \beta_{\text{ext}} dz$, and hence the cloud albedo as $A_c = \tau_c/(2 + \tau_c)$ (e.g., Bohren, 1987). Further note that β_{ext} includes the term $(1 - g)$ to account for the increasing degree of backward scattering typical for particles in the Mie regime, which tends to increase A_c (e.g., Schwartz et al., 2017).

Figure 5 shows the contribution of haze particles to the total β_{ext} . Irrespective of the temporal changes, we see that the contribution of haze particles increases with particle concentration (line color) and dry aerosol size (line pattern). While the prior is expected from the dependency of β_{ext} on n and hence N_a , the latter is a result of the equilibrium radii that haze particles attain, which are proportional to the dry aerosol size (e.g., Sedunov et al., 1974). During the mixing, the contribution of haze particles increases almost constantly until saturation is

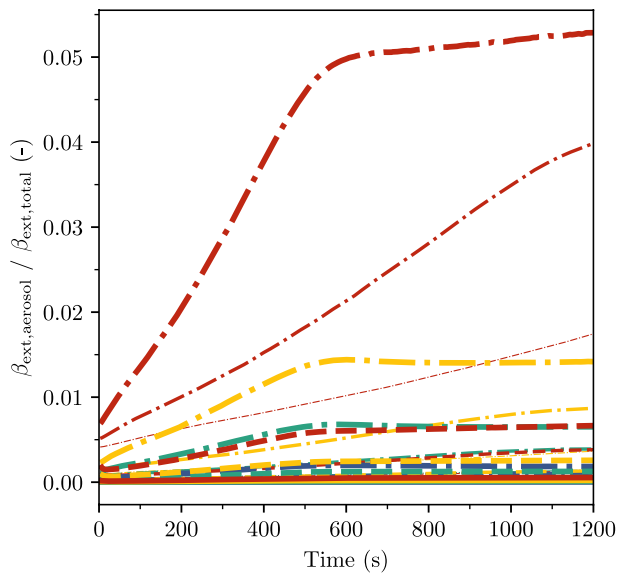


Figure 5. Relative contributions of haze particles to the total extinction. See Figure 2 for line labels.

reached (cf. Figure 2a). And once the domain is saturated, the contribution of haze particles to β_{ext} remains almost constant. This behavior can be related to the increasing N_a during the mixing, but also again to the haze particle equilibrium radii, which are also proportional to the saturation, allowing the haze to attain larger sizes in a saturated environment. This also explains the dependency on ϵ (line thickness): in a more turbulent environment, mixing progresses faster which allows the haze to attain their larger equilibrium radius more quickly.

While this analysis indeed shows that the contribution of haze particles to β_{ext} can be neglected during the actual mixing process, the contribution of surviving haze particles after the mixing process can reach up to 5% and thus buffers the negative albedo bias due to inhomogeneous mixing. In fact, further sensitivity studies with a larger entrainment fraction (not shown) indicate that the contribution of haze particles increases for more dilute clouds, that is, thin clouds which are most susceptible to the negative albedo bias from inhomogeneous mixing (cf. Chosson et al., 2007), suggesting a much more substantial buffering effect.

6. Summary and Conclusions

In this study, we investigated the influence of aerosol on the character of small-scale cloud-environment mixing, focusing on changes in the droplet size distribution and cloud optical properties when aerosol particles are treated in full detail. The results presented in this study were created using detailed Lagrangian cloud and aerosol microphysics coupled with a high resolution statistical turbulence model.

1. The so-called IHMD (e.g., Andrejczuk et al., 2009), which is frequently applied to determine or parametrize the character of small-scale mixing, was shown to be highly sensitive to minor changes in the radius used to separate haze particles from cloud droplets. The comparison of different separation radii to the critical activation radius, which was calculated from Köhler theory for each particle individually, showed that the choice of the separation radius can bias the estimated mixing character toward a more homogeneous scenario. This effect was found to become significant for situations in which sufficiently large aerosol particles can sustain haze particles with radii larger than $\mathcal{O}(1 \mu\text{m})$, for example, sea salt particles frequently found in maritime conditions (Jaenicke, 1993). This bias can become problematic for the analysis of observational data, since typical cloud droplet measurement instruments cannot distinguish between activated cloud droplets or deactivated haze particles, but use a minimal detection radius or a fixed separation radius applied in data analysis, for example, the CAS (0.2 μm), FSSP (0.7 μm), or PVM (1.5 μm). Thus, we suggest to test the sensitivity of observationally determined IHMDs against the applied separation radius.
2. A second process that has consequences on the mixing character is Ostwald ripening, that is, the growth of the largest particles on the expense of the smallest due to the interplay of particle curvature and aerosol solubility (e.g., Korolev, 1995). While its contribution can be neglected during the actual mixing process, as soon as the domain is saturated, it becomes unmissable, and appears as inhomogeneous mixing. Thus, the interpretation of a diagnosed mixing character needs to include the possibility for Ostwald ripening, biasing observations toward inhomogeneous mixing. Note that this effect is probably limited to the top of stratocumulus clouds, where low vertical velocities limit the production of supersaturation, which favors the occurrence of Ostwald ripening.
3. The study is concluded by investigating the changes of cloud optical properties during the mixing process, including the effects of haze particles. It is found that especially once mixing is finished, the haze contribution to the extinction coefficient can become important if the underlying aerosol particles are large and their number concentration is high. While previous studies have shown a substantial decrease in the cloud albedo due to inhomogeneous mixing (Chosson et al., 2007), the correct consideration of haze particles buffers this effect.

All in all, this study showed that small-scale mixing processes cannot be treated properly without taking the effects of aerosol and hence haze particles into account. Previous concepts that only consider the category of cloud droplets have been shown to be too simple, causing potentially misleading conclusions from observations and simulations. It is obvious that, with more detailed cloud microphysical models and the ability of probes

detecting even particles much smaller than $\mathcal{O}(1 \mu\text{m})$, better ways to determine the degree of inhomogeneous mixing are necessary.

Data Availability Statement

The simulation data produced for this study is publicly available (Kainz & Hoffmann, 2023).

Acknowledgments

This work was supported by the Emmy-Noether program of the German Research Foundation (DFG) under Grant HO 6588/1-1. Open Access funding enabled and organized by Projekt DEAL.

References

- Andrejczuk, M., Grabowski, W. W., Malinowski, S. P., & Smolarkiewicz, P. K. (2009). Numerical simulation of cloud–clear air interfacial mixing: Homogeneous versus inhomogeneous mixing. *Journal of the Atmospheric Sciences*, *66*(8), 2493–2500. <https://doi.org/10.1175/2009JAS2956.1>
- Baker, M. B., Corbin, R. G., & Latham, J. (1980). The influence of entrainment on the evolution of cloud droplet spectra: I. A model of inhomogeneous mixing. *Quarterly Journal of the Royal Meteorological Society*, *106*(449), 581–598. <https://doi.org/10.1002/qj.49710644914>
- Baker, M. B., & Latham, J. (1979). The evolution of droplet spectra and the rate of production of embryonic raindrops in small cumulus clouds. *Journal of the Atmospheric Sciences*, *36*(8), 1612–1615. [https://doi.org/10.1175/1520-0469\(1979\)036\(1612:TEODSA\)2.0.CO;2](https://doi.org/10.1175/1520-0469(1979)036(1612:TEODSA)2.0.CO;2)
- Baumgardner, D., Jonsson, H., Dawson, W., O'Connor, D., & Newton, R. (2001). The cloud, aerosol and precipitation spectrometer: A new instrument for cloud investigations. *Atmospheric Research*, *59–60*, 251–264. [https://doi.org/10.1016/S0169-8095\(01\)00119-3](https://doi.org/10.1016/S0169-8095(01)00119-3)
- Beard, K. V. (1976). Terminal velocity and shape of cloud and precipitation drops aloft. *Journal of the Atmospheric Sciences*, *33*(5), 851–864. [https://doi.org/10.1175/1520-0469\(1976\)033\(0851:TVASOC\)2.0.CO;2](https://doi.org/10.1175/1520-0469(1976)033(0851:TVASOC)2.0.CO;2)
- Bohren, C. F. (1987). Multiple scattering of light and some of its observable consequences. *American Journal of Physics*, *55*(6), 524–533. <https://doi.org/10.1119/1.15109>
- Brenguier, J.-L., Rodi, A. R., Gordon, G., & Wechsler, P. (1993). Real-time detection of performance degradation of the forward-scattering spectrometer probe. *Journal of Atmospheric and Oceanic Technology*, *10*(1), 27–33. [https://doi.org/10.1175/1520-0426\(1993\)010\(0027:RTDOPD\)2.0.CO;2](https://doi.org/10.1175/1520-0426(1993)010(0027:RTDOPD)2.0.CO;2)
- Burnet, F., & Brenguier, J.-L. (2007). Observational study of the entrainment–mixing process in warm convective clouds. *Journal of the Atmospheric Sciences*, *64*(6), 1995–2011. <https://doi.org/10.1175/JAS3928.1>
- Çelik, F., & Marwitz, J. D. (1999). Droplet spectra broadening by ripening process. Part I: Roles of curvature and salinity of cloud droplets. *Journal of the Atmospheric Sciences*, *56*(17), 3091–3105. [https://doi.org/10.1175/1520-0469\(1999\)056\(3091:DSBRRP\)2.0.CO;2](https://doi.org/10.1175/1520-0469(1999)056(3091:DSBRRP)2.0.CO;2)
- Chosson, F., Brenguier, J.-L., & Schüller, L. (2007). Entrainment–mixing and radiative transfer simulation in boundary layer clouds. *Journal of the Atmospheric Sciences*, *64*(7), 2670–2682. <https://doi.org/10.1175/JAS3975.1>
- Geoffroy, O., Brenguier, J.-L., & Burnet, F. (2010). Parametric representation of the cloud droplet spectra for less warm bulk microphysical schemes. *Atmospheric Chemistry and Physics*, *10*(10), 4835–4848. <https://doi.org/10.5194/acp-10-4835-2010>
- Gerber, H. E., Arends, B. G., & Ackerman, A. S. (1994). New microphysics sensor for aircraft use. *Atmospheric Research*, *31*(4), 235–252. [https://doi.org/10.1016/0169-8095\(94\)90001-9](https://doi.org/10.1016/0169-8095(94)90001-9)
- Hagen, D. E. (1979). A numerical cloud model for the support of laboratory experimentation. *Journal of Applied Meteorology and Climatology*, *18*(8), 1035–1043. [https://doi.org/10.1175/1520-0450\(1979\)018\(1035:ANCMFT\)2.0.CO;2](https://doi.org/10.1175/1520-0450(1979)018(1035:ANCMFT)2.0.CO;2)
- Hoffmann, F. (2020). Effects of entrainment and mixing on the Wegener–Bergeron–Findeisen process. *Journal of the Atmospheric Sciences*, *77*(6), 2279–2296. <https://doi.org/10.1175/JAS-D-19-0289.1>
- Hoffmann, F., Mayer, B., & Feingold, G. (2022). A parameterization of interstitial aerosol extinction and its Application to marine cloud brightening. *Journal of the Atmospheric Sciences*, *79*(11), 2849–2862. <https://doi.org/10.1175/JAS-D-22-0047.1>
- Hoffmann, F., Raasch, S., & Noh, Y. (2015). Entrainment of aerosols and their activation in a shallow cumulus cloud studied with a coupled LCM–LES approach. *Atmospheric Research*, *156*, 43–57. <https://doi.org/10.1016/j.atmosres.2014.12.008>
- Jaenicke, R. (1993). Chapter 1 tropospheric aerosols. In P. V. Hobbs (Ed.), *Aerosol–cloud–climate interactions* (Vol. 54, pp. 1–31). Academic Press. [https://doi.org/10.1016/S0074-6142\(08\)60210-7](https://doi.org/10.1016/S0074-6142(08)60210-7)
- Kainz, J., & Hoffmann, F. (2023). The effects of aerosol on small-scale cloud–environment mixing: Implications for observing inhomogeneous mixing [Dataset]. Zenodo. <https://doi.org/10.5281/zenodo.7503463>
- Kerstein, A. R. (1988). A linear–eddy model of turbulent scalar transport and mixing. *Combustion Science and Technology*, *60*(4–6), 391–421. <https://doi.org/10.1080/00102208808923995>
- Köhler, H. (1936). The nucleus in and the growth of hygroscopic droplets. *Transactions of the Faraday Society*, *32*(0), 1152–1161. <https://doi.org/10.1039/TF9363201152>
- Kokhanovsky, A. (2004). Optical properties of terrestrial clouds. *Earth-Science Reviews*, *64*(3), 189–241. [https://doi.org/10.1016/S0012-8252\(03\)00042-4](https://doi.org/10.1016/S0012-8252(03)00042-4)
- Korolev, A. V. (1995). The influence of supersaturation fluctuations on droplet size spectra formation. *Journal of the Atmospheric Sciences*, *52*(20), 3620–3634. [https://doi.org/10.1175/1520-0469\(1995\)052\(3620:TIOSFO\)2.0.CO;2](https://doi.org/10.1175/1520-0469(1995)052(3620:TIOSFO)2.0.CO;2)
- Korolev, A. V., Khain, A., Pinsky, M., & French, J. (2016). Theoretical study of mixing in liquid clouds—Part 1: Classical concepts. *Atmospheric Chemistry and Physics*, *16*(14), 9235–9254. <https://doi.org/10.5194/acp-16-9235-2016>
- Krueger, S. K., & Tölle, M. H. (2014). Effects of entrainment and mixing on droplet size distributions in warm cumulus clouds. *Journal of Advances in Modeling Earth Systems*, *6*(2), 281–299. <https://doi.org/10.1002/2012MS000209>
- Kumar, B., Schumacher, J., & Shaw, R. A. (2014). Lagrangian mixing dynamics at the cloudy–clear air interface. *Journal of the Atmospheric Sciences*, *71*(7), 2564–2580. <https://doi.org/10.1175/JAS-D-13-0294.1>
- Lasher-Trapp, S. G., Cooper, W. A., & Blyth, A. M. (2005). Broadening of droplet size distributions from entrainment and mixing in a cumulus cloud. *Quarterly Journal of the Royal Meteorological Society*, *131*(605), 195–220. <https://doi.org/10.1256/qj.03.199>
- Latham, J., & Reed, R. L. (1977). Laboratory studies of the effects of mixing on the evolution of cloud droplet spectra. *Quarterly Journal of the Royal Meteorological Society*, *103*(436), 297–306. <https://doi.org/10.1002/qj.49710343607>
- Lehmann, K., Siebert, H., & Shaw, R. A. (2009). Homogeneous and inhomogeneous mixing in cumulus clouds: Dependence on local turbulence structure. *Journal of the Atmospheric Sciences*, *66*(12), 3641–3659. <https://doi.org/10.1175/2009JAS3012.1>
- Lehmann, K., Siebert, H., Wendisch, M., & Shaw, R. A. (2007). Evidence for inertial droplet clustering in weakly turbulent clouds. *Tellus Series B Chemical and Physical Meteorology*, *59*(1), 57–65. <https://doi.org/10.1111/j.1600-0889.2006.00229.x>

- Lilly, D. K. (1968). Models of cloud-topped mixed layers under a strong inversion. *Quarterly Journal of the Royal Meteorological Society*, 94(401), 292–309. <https://doi.org/10.1002/qj.49709440106>
- Lu, C., Liu, Y., Niu, S., Krueger, S., & Wagner, T. (2013). Exploring parameterization for turbulent entrainment-mixing processes in clouds. *Journal of Geophysical Research: Atmospheres*, 118(1), 185–194. <https://doi.org/10.1029/2012JD018464>
- Lu, C., Niu, S., Liu, Y., & Vogelmann, A. M. (2013). Empirical relationship between entrainment rate and microphysics in cumulus clouds. *Geophysical Research Letters*, 40(10), 2333–2338. <https://doi.org/10.1002/grl.50445>
- V. Masson-Delmotte, P. Zhai, A. Pirani, S. L. Connors, C. Péan, S. Berger, et al. (Eds.) (2021). *Climate Change 2021: The Physical Science Basis. Contribution of Working Group I to the Sixth Assessment Report of the Intergovernmental Panel on Climate Change*. Cambridge University Press. <https://doi.org/10.1017/9781009157896>
- Mellado, J. P. (2017). Cloud-top entrainment in stratocumulus clouds. *Annual Review of Fluid Mechanics*, 49(1), 145–169. <https://doi.org/10.1146/annurev-fluid-010816-060231>
- Mitchell, D. L. (2000). Parameterization of the mie extinction and absorption coefficients for water clouds. *Journal of the Atmospheric Sciences*, 57(9), 1311–1326. [https://doi.org/10.1175/1520-0469\(2000\)057<1311:POTMEA>2.0.CO;2](https://doi.org/10.1175/1520-0469(2000)057<1311:POTMEA>2.0.CO;2)
- Rogers, R., & Yau, M. (1989). *A short course in cloud physics*. Butterworth-Heinemann.
- Schwartz, S. E., Huang, D., & Vladutescu, D. V. (2017). High-resolution photography of clouds from the surface: Retrieval of optical depth of thin clouds down to centimeter scales. *Journal of Geophysical Research: Atmospheres*, 122(5), 2898–2928. <https://doi.org/10.1002/2016JD025384>
- Sedunov, Yu. S.I., Greenberg, P., & Lederman, D. (1974). *Physics of drop formation in the atmosphere*. Wiley. Retrieved from <https://books.google.de/books?id=8TRRAAAMAAJ>
- Wood, R. (2012). Stratocumulus clouds in: Monthly weather review (Vol. 140, p. 8). Retrieved from <https://journals.ametsoc.org/view/journals/mwre/140/8/mwr-d-11-00121.1.xml>
- Wood, R., Irons, S., & Jonas, P. R. (2002). How important is the spectral ripening effect in stratiform boundary layer clouds? Studies using simple trajectory analysis. *Journal of the Atmospheric Sciences*, 59(18), 2681–2693. [https://doi.org/10.1175/1520-0469\(2002\)059<2681:HIITSR>2.0.CO;2](https://doi.org/10.1175/1520-0469(2002)059<2681:HIITSR>2.0.CO;2)
- Xue, Y., Wang, L.-P., & Grabowski, W. W. (2008). Growth of cloud droplets by turbulent collision-coalescence. *Journal of the Atmospheric Sciences*, 65(2), 331–356. <https://doi.org/10.1175/2007JAS2406.1>
- Yamaguchi, T., & Randall, D. A. (2012). Cooling of entrained parcels in a large-eddy simulation. *Journal of the Atmospheric Sciences*, 69(3), 1118–1136. <https://doi.org/10.1175/JAS-D-11-080.1>

Erratum

The originally published version of this article contained a typographical error. In the eighth sentence of the third paragraph of Section 3, the word “Eqaution” should be “Equation.” The error has been corrected, and this may be considered the authoritative version of record.